



Evaluation of the mirror surface figure error based on the SlopeRMS

Wang Fu-guo^{*}, An Qi-chang¹, Yang Fei¹

Changchun Institute of Optics, Fine Mechanics and Physics, Chinese Academy of Sciences, Photoelectric Detection Department, Dong Nanhu Road 3888, Changchun 130033, Jilin, China

ARTICLE INFO

Article history:

Received 30 November 2014
 Accepted 29 September 2015

Keywords:

Mirror surface figure error
 SlopeRMS
 Zernike polynomial
 Power spectrum

ABSTRACT

The slope of the root mean square (SlopeRMS) can be applied to evaluate mid-spatial frequency mirror surface errors for larger aperture mirrors. In this paper, the SlopeRMS is analyzed from three different perspectives. First, the relationship between the SlopeRMS and the basis polynomials is discussed, and the mathematic relationship between the SlopeRMS and the standard orthogonal basis was obtained. Second, the SlopeRMS is analyzed by applying the Wiener process, with the results indicating that the ideal mirror surface error obeys the Gauss distribution law. Then, a power spectrum analysis method based on the SlopeRMS is proposed. The discrete random variables for describing the coma, astigmatism and quatrefoil were analyzed and the spectral energy distribution for the Zernike polynomials is discussed. Finally, by processing the error data of the Thirty Meter Telescope tertiary mirror surface figure, the frequency domain energy distribution of the actual mirror surface figure was obtained.

© 2015 Elsevier GmbH. All rights reserved.

1. Introduction

A variety of methods exists to evaluate the surface figure error of reflective mirrors. As a traditional evaluation method, the root mean square (RMS) is typically used to describe the surface figure error of small aperture mirrors. Because the size of the grinding tools and the size of the optical components are similar, it can be applied to describe the simplest optical characteristics [1,2].

However, for large aperture reflective mirrors, this evaluation method faces several limitations. First, the small size of the grinding tools that are employed to polish the large aperture mirror will produce sub-aperture scale and mid-spatial frequencies, especially for aspheric surfaces and free surfaces. Particularly the grinding smoothness depends on a uniform distribution caused by the tools and the holding pressure time. Second, a multi-point support is always used for large aperture mirrors. As the number of support points increases, the mirrors will become more prone to mid-spatial frequencies. These mid-spatial frequencies produced by fringe irregularities are several times smaller than the optical element aperture, but larger than the surface's precision structure, i.e. the mirror surface roughness [3,4].

For different spatial frequency mirror surface figure errors, different evaluation methods produce different results. Fig. 1 shows a schematic illustration of two different optical surface figure errors. The optical surface of mirror A exhibits low frequency errors, while

the optical surface of mirror B shows high frequency errors. When using the traditional RMS optical surface evaluation method, the RMS value is relatively large for mirror A, and relatively small for mirror B, and, consequentially, mirror A is unqualified, and mirror B is qualified. However, mirror A mainly exhibits low frequency errors, which can be easily corrected by applying adaptive optics, whereas the high frequency errors of mirror B are difficult to correct by adaptive optics. Therefore, the RMS evaluation method has its limitations for large aperture mirrors. In contrast, if using the slope of the root mean square (SlopeRMS) to evaluate the mirror surface error, the SlopeRMS value obtained for mirror A is small, and the SlopeRMS obtained for mirror B is large. Thus, mirror A is qualified, and mirror B is unqualified [1–4].

For large aperture mirrors, the surface figure test and evaluation directly affects the manufacturing accuracy and imaging quality [5,6]. The RMS test shows obvious shortcomings for evaluating large aperture mirrors. In recent years, some researchers therefore proposed using the SlopeRMS to evaluate the mirror surface error in the time domain. Although it can control rigid body displacements and reflect a wide range of roughnesses [7,8], for small scale shakes, there will be dramatic fluctuations. Therefore, an analysis based on the frequency-domain is necessary.

2. Mathematical analysis of the SlopeRMS

2.1. SlopeRMS and basis polynomials

Low order wave front errors are always fitted by basis polynomials. More precisely, the wave front error can be described by discrete index basis polynomials:

* Corresponding author. Tel.: +86 0431 86708871-613.

E-mail address: wfg109@163.com (W. Fu-guo).

¹ Tel.: +86 0431 86708871-613.

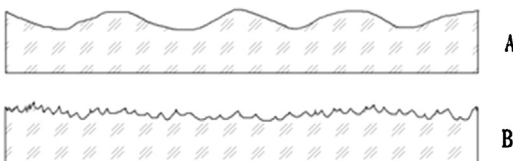


Fig. 1. Schematic illustration of two different mirror surface figures with (A) low-frequency errors and (B) high-frequency errors, respectively.

$$\Phi(m, n) = \sum a_{uv} W_{uv}(m, n) \quad (1)$$

where a_{uv} is the basis fitting coefficient and $W_{uv}(m, n)$ denotes the discrete index basis.

For a $N \times N$ sampling aperture, $W_{uv}(m, n)$ can be expressed by

$$W_{uv}(m, n) = \frac{1}{N \times N} \exp \left[\frac{2\pi j}{N} (um + vn) \right] \quad (2)$$

For convenience, only the imaginary component is considered in the one dimensional case, resulting in a standard sine polynomial. If the wave front error energy is constant, the RMS cannot be used to comprehensively reflect its dynamic performance. Therefore, the SlopeRMS is applied to address this problem:

$$\Phi = A \sin(2\pi f x) \quad (3)$$

with

$$\begin{aligned} (\nabla \Phi)^2 &= (\nabla A \sin(2\pi f x))^2 \\ &= 4A^2 \pi^2 f^2 \cos^2(2\pi f x) \\ \langle \nabla \Phi^2 \rangle &= \frac{2A^2 \pi f \int_0^{1/f} \cos^2(2\pi f x) 2\pi f dx}{1/f} \\ &= 2A^2 \pi^2 f^2 \end{aligned} \quad (4)$$

For the standard sine polynomial in Eq. (3), the wave front error is constant, i.e. $\text{RMS}_\Phi = A$. Its SlopeRMS can be expressed by Eq. (6):

$$\Phi = \sqrt{2} A \sin(2\pi f x) \quad (5)$$

$$\text{slopeRMS} = \sqrt{2} \pi f A_{(2)} \quad (6)$$

It is generally assumed that the wave front error is a linear combination of two standard sine polynomials, as illustrated by Fig. 2, and its SlopeRMS can be expressed as follows:

$$\begin{aligned} \Phi &= \alpha \sqrt{2} A \sin(2\pi f x) + \beta \sqrt{2} A \sin(2\pi f x) \\ \text{slopeRMS}^2 &= \left(\sqrt{2\alpha^2 + 8\beta^2 \pi A f} \right)^2 = \alpha^2 2f^2 A^2 + \beta^2 8f^2 A^2 \end{aligned}$$

An extension of this construction to rank N yields:

$$\text{slopeRMS}^2 = \sum_i c_i^2 \text{slopeRMS}_i^2 \quad (7)$$

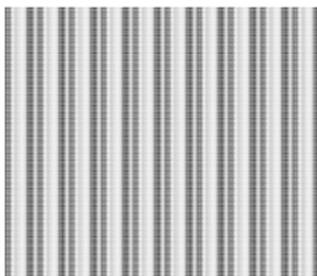


Fig. 2. Illustration of the multiplied wave front error.

This suggests that, if the wave front error is expressed by a standard orthogonal basis such as a standard sine polynomial, every item's SlopeRMS can be calculated individually, with the total SlopeRMS then obtained by summation. In the actual engineering application, some item's SlopeRMS can be first calculated as well, and then the total SlopeRMS can be obtained.

2.2. Ideal surface figure and Wiener process

For the surface figure of a reflective mirror, even for an absolutely ideal surface, the measurement instrument will produce an unavoidable error that will affect the mirror surface data; on the other hand, because of other uncontrollable factors (pressure disc jitter, thermal motion of magnetron fluid particles, random motion of beam particles), the actual surface figure will contain irregular fluctuations after the mirror has been polished.

The mathematical model of the Wiener Process was proposed by Einstein to analyze Brownian movement, essentially capturing the irregular movement by using a set of mathematical rules. This paper will analyze the mirror surface figure by referring to the Wiener process.

According to the basic assumptions of the Wiener process, in the measurement range, the mirror surface slope is zero at the starting point, whereas the surface slope has the following properties:

- (1) Each coordinate component of the mirror surface slope $w(d_1) - w(u_1), w(d_2) - w(u_2), \dots, w(d_n) - w(u_n)$ is independent. For one of the components, it is denoted as $w(l)$, while for arbitrary mutually disjoint regions, it is denoted as $[d_1, u_1], [d_2, u_2], \dots, [d_n, u_n]$.
- (2) The ideal error should be symmetrically distributed, so that $E\{w(l)\} = 0$.
- (3) The $w(l + \Delta) - w(l)$ distribution does not depend on l . Furthermore, $\sigma^2(\Delta) = E\{(w(l + \Delta) - w(l))^2\}$ exists and is the continuous function of Δ . As a result

$$\Phi(l, \lambda) = E\{e^{i\lambda w(l)}\} = \int_{-\infty}^{+\infty} e^{i\lambda x} f(l, x) dx \quad (8)$$

and

$$\sigma^2(l) = E\{[w(l) - w(0)]^2\} = E\{w^2(l)\} = \int_{-\infty}^{+\infty} x^2 f(l, x) dx \quad (9)$$

Then,

$$\begin{aligned} \sigma^2(l+s) &= E\{[w(l+s) - w(l) + w(l) - w(0)]^2\} \\ &= E\{[w(l+s) - w(l)]^2\} + E\{w^2(l)\} = \sigma^2(s) + \sigma^2(l) \end{aligned} \quad (10)$$

$$\sigma^2(l) = Cl(C > 0) \quad (11)$$

$$\Phi(l+s, \lambda) - \Phi(l, \lambda) = \Phi(l, \lambda) E\{e^{i\lambda w(s) - w(0)} - 1\} \quad (12)$$

and

$$e^{iv} \approx 1 + iv - \frac{v^2}{2} \quad (13)$$

Therefore:

$$\frac{\Phi(l+s, \lambda) - \Phi(l, \lambda)}{s} \approx \frac{1}{2} \lambda^2 \Phi(l, \lambda) C \quad (14)$$

If $s \rightarrow 0$, then

$$\frac{\partial \Phi(l, \lambda)}{\partial l} = -\frac{1}{2} \lambda^2 \Phi(l, \lambda) C \quad (15)$$

Since $\Phi(0, \lambda) = 1$

we finally obtain:

$$\Phi(l, \lambda) = \int_{-\infty}^{+\infty} e^{i\lambda x} \frac{1}{\sqrt{2\pi Cl}} e^{-\frac{x^2}{2Cl}} dx \quad (16)$$

From Eq. (4), it can be concluded that the SlopeRMS of the ideal mirror surface figure error should obey the Gauss distribution law and, consequentially, the SlopeRMS energy should obey the equipartition law.

2.3. SlopeRMS power spectrum analysis

Suppose there is a stochastic process $\{X(t), t \in T\}$. For every t , the first moment $E[x_1]$ and the second moment $E[x_2]$ exists. Therefore, we define $\{X(t), t \in T\}$ as the second moment process.

Assuming that there is no destruction, the measured mirror surface slope will never be infinite. Since the first moment $E[x_1]$ and the second moment $E[x_2]$ always exist, the random series describing the mirror surface figure wave front error is a second moment process.

Considering the coefficient $R(\theta(x+r), \theta(x))$ for a second moment process, by applying the Cauchy–Schwarz-Law, we obtain:

$$\begin{aligned} & R^2(\theta(x+r), \theta(x)) \\ &= \left\{ E[\theta(x+r)\theta(x)] \right\}^2 \leq E[\theta^2(x+r)] E[\theta^2(x)] < +\infty \end{aligned} \quad (17)$$

Thus the coefficient $R(\theta(x+r), \theta(x))$ for the second moment process always exists, and thereby satisfies the condition for Fourier transformation, i.e. it can be processed to perform a power spectrum analysis. Furthermore, due to its invariability and time-invariance, the expectation can be regarded as a steady state process.

The power spectrum density (PSD) is defined as follows:

$$\begin{aligned} S(\omega) &= \sum_{-\infty}^{+\infty} R(m) e^{-j\omega} \\ &= \sum_{-\infty}^{+\infty} E[x(n)x^*(n+m)] e^{-j\omega} \end{aligned} \quad (18)$$

For a random series describing the reflective mirror surface wave front error, its self-correction function can be expressed by

$$R(r) = \langle \theta(x+r)\theta(x) \rangle_x \quad (19)$$

and the self-power spectrum density is given by

$$s(\varpi) = F(R(r)) = F(\langle \theta(x+r)\theta(x) \rangle_x) \quad (20)$$

The previous two sections suggest that the system wave front error is composed of a low order wave front error and a high order noise (with an almost ideal Gauss distribution). Then, by applying the methods mentioned above, the standard Zernike polynomials for describing the coma, astigmatism and quatrefoil were analyzed, and the results are shown in Figs. 3–5, respectively.

$$\begin{aligned} S(\omega) &= \sum_{-\infty}^{+\infty} R(m) e^{-j\omega} \\ &= \sum_{-\infty}^{+\infty} E[x(n)x^*(n+m)] e^{-j\omega} \end{aligned} \quad (21)$$

$$R(r) = \langle \theta(x+r)\theta(x) \rangle_x \quad (22)$$

$$s(\varpi) = F(R(r)) = F(\langle \theta(x+r)\theta(x) \rangle_x) \quad (23)$$

The power spectrum analysis reveals that the energy peaks are shifted to higher frequencies with increasing order of the

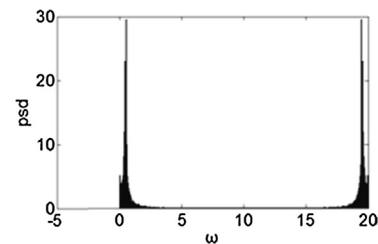


Fig. 3. Coma power spectrum.

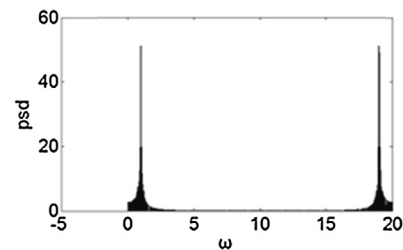


Fig. 4. Astigmatism power spectrum.

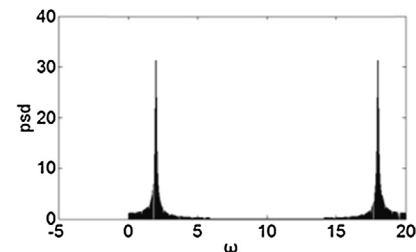


Fig. 5. Quatrefoil power spectrum.

Zernike polynomials. At the same time, the frequency width also increases. After the data has been normalized, the basic aberration of the actual surface figure power spectrum can be analyzed, cp. Figs. 3–5.

3. Application of the SlopeRMS method

The TMT (Thirty Meter Telescope) is an optical and infrared telescope. Its tertiary mirror is a 3594 mm × 2536 mm elliptical flat mirror with a thickness of 100 mm. Because the TMT primary segment mirror and deformable mirror are able to correct the tertiary mirror surface figure error, if the traditional RMS method is used to evaluate the TMT tertiary mirror surface figure, it cannot generally and objectively reflect the requirements of the tertiary mirror [9,10].

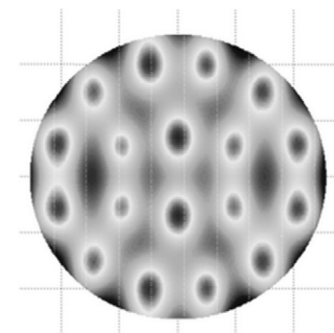


Fig. 6. Tertiary mirror surface figure error (tilt removed).

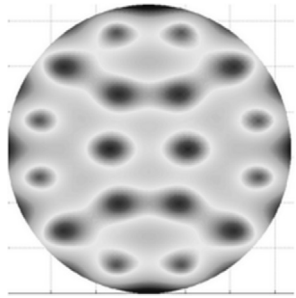


Fig. 7. The normalized tertiary mirror surface figure error.

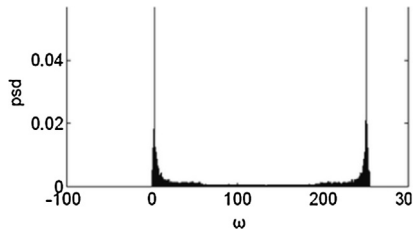


Fig. 8. Power spectrum density of the TMT tertiary mirror.

An 18-point support structure is used for the TMT tertiary mirror and the resulting surface figure error is shown in Fig. 6. The error was normalized to a unit circle, as shown in Fig. 7, and its power spectrum density is shown in Fig. 8.

Fig. 8 indicates that the main deformation of the TMT tertiary mirror is smaller than the coma component (defocus and astigmatism). However, in order to perform an ideal finite element analysis, the high frequency contribution is considered to be zero. It is advantageous to differentiate the system aberration by applying the frequency domain analysis method, as well as to evaluate the surface figure error.

For the TMT tertiary mirror surface figure error with removed defocus and astigmatism, a SlopeRMS of $0.98 \mu\text{rad}$ was obtained. Then, from Eq. (2), the frequency $f_0 = (\text{slopeRMS}/\sqrt{2\pi}A)$, which is defined as the system limiting frequency, can be obtained.

4. Summary

The SlopeRMS has been mathematically analyzed from three different perspectives, some basic characteristics have been obtained, and a power spectrum analysis method has been proposed. The discrete random series for the Zernike polynomials was analyzed by using the SlopeRMS method, and the spectrum energy distribution for the Zernike polynomials was obtained. Finally, the TMT tertiary mirror surface figure error was analyzed by applying the SlopeRMS method, indicating that this method is superior for larger aperture mirror surface figures.

Acknowledgements

This research was carried out at the National Natural Science Foundation of China. The author gratefully acknowledges the support of the CTMT colleagues. And the author would like to acknowledge PhD Yang Liu for her review and helpful comments.

References

- [1] Y. Bi, J. Zhai, J.H. Wu, Q.Q. Hu, One method for mirror surface figure treatment in optical instrument, *Opt. Tech.* 35 (1) (2009) 10–17 (in Chinese).
- [2] D. Wang, H.B. Yang, C.Z.H. Chen, Computer simulation of the optical surface, *Comput. Simul.* 24 (2) (2007) 298–301 (in Chinese).
- [3] P.J. Van Zwol, G. Palasantzas, Th.J.M. De Hosson, Roughness corrections to the Casimir force: the importance of local surface slope, *Appl. Phys. Lett.* 91 (2007) 144108-1–144108-3.
- [4] Dierking Wolfgang, RMS slope of exponentially correlated surface roughness for radar applications, *IEEE Trans. Geosci. Remote Sens.* 38 (May (3)) (2000) 1451–1454.
- [5] Zhelem Ross, Specification of optical surface accuracy using the structure function, *SPIE* 8083 (2011), 808310-1–808310-10.
- [6] Anastacia M. Hvise, James H. Burge, Structure function analysis of mirror fabrication and support errors, *SPIE* 6671 (2007), 66710A-1–66710A-110.
- [7] Yuchun Wang, Heyi Sun, Wenyang Tang, Chongran Jiang, Siqing Tian, Angle subdivision approach algorithm for conicoid profile error evaluation, *Opt. Precis. Eng.* 22 (6) (2014) 1606–1612 (in Chinese).
- [8] Kuntao Huang, Fengzhou Fang, Hu Gong, Effec of surface microscopic topology generated by ultra-precision turning on optical characteristics, *Opt. Precis. Eng.* 21 (1) (2013) 10–107 (in Chinese).
- [9] Tertiary Mirror Surface Figure Specification. TMT. Opt. SPIE. 12.001. DRF02.2012.
- [10] Wang Fu-guo, Qichang An, Evaluation of mirror surface figure for TMT based on SlopeRMS, *Opt. Precis. Eng.* 22 (5) (2014) 1171–1175 (in Chinese).